Table S1. WRF-Chem model basic configuration in this study.

Configuration	Option/Setting	Reference
Gas-phase chemistry	Carbon Bond Mechanism Z (CBMZ)	Zaveri and Peters (1999)
Aerosol	Model for Simulating Aerosol Interactions and Chemistry (MOSAIC), 4-bin	Zaveri et al. (2008)
Microphysics	Morrison two-moment	Morrison and Gettelman (2008)
Shortwave and longwave	Rapid Radiative Transfer Model for GCMs (RRTMG)	Iacono et al. (2008)
Land surface model	Noah	Chen and Dudhia (2001); Ek et al. (2003)
Planetary boundary layer	Mellor–Yamada–Nakanishi–Niino (MYNN)	Nakanishi and Niino (2006)
Meteorological initial conditions (IC) and lateral boundary conditions (LBC)	NCEP FNL Operational Global Analysis (6-hourly, $1^\circ \times 1^\circ$)	National Centers for Environmental Prediction, National Weather Service, NOAA, U.S. Department of Commerce (2000)
Chemical LBC	CESM2.2 CAM-Chem fields (6-hourly, $0.9^\circ \times 1.25^\circ$)	Tilmes et al. (2022)
Anthropogenic emissions	MEIC v2.0	Li et al. (2017); Geng et al. (2024)
Biogenic emissions	MEGAN (as implemented in WRF-Chem) with updated input datasets	Guenther et al. (2012); Guenther (2024)
Land-use dataset	Default WRF land-use replaced with GLC_FCS30-2020 (30 m)	
citetLiu2020GLC,Zhang2021GLC		
Nesting	Two nested domains (d01, d02)	see Fig. 2a in the main text for details
Horizontal grid spacing	d01: 9 km; d02: 3 km	see Fig. 2a in the main text for details
Vertical levels	34 levels	–
Model top	$\sim$50 hPa	–
Time step	30 s	–
Ensemble size	80 members	–

The basic WRF-Chem configuration in this study is shown in Table S1. In particular, anthropogenic emissions in the ALL run simulation were prescribed using version 2.0 of the Multi-resolution Emission Inventory for China (MEIC; Li et al., 2017; Geng et al., 2024) and processed with the meic2wrf preprocessor Fan et al., 2020 to generate WRF-Chem-ready emission fields for major aerosol precursor species. Biogenic emissions were computed using the Model of Emissions of Gases and Aerosols from Nature (MEGAN; Guenther et al., 2012; Guenther, 2024) as implemented in WRF-Chem. To better represent present-day urbanization, the leaf area index (LAI) and plant functional type (PFT) used by MEGAN were updated. LAI was recalculated using the MODIS Terra 16-day 250 m vegetation index product (MOD13Q1, version 6.1; Didan, 2021), and PFT was updated using the GLC_FCS30-2020 dataset.

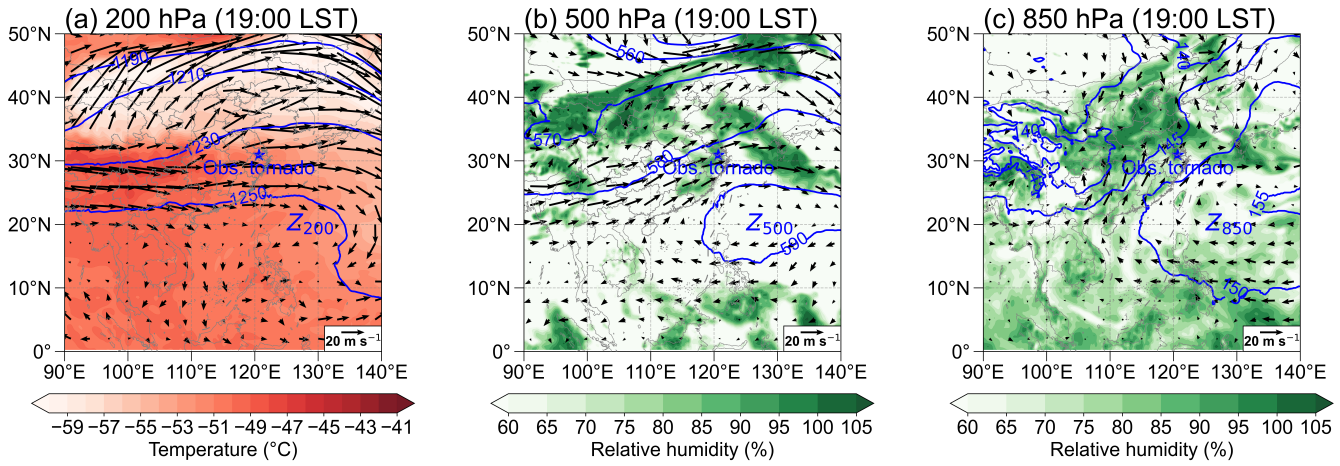

Figure S1. Large-scale environment conditions. (a) Temperature (shading; unit: °C), geopotential height (blue contours; unit: dagpm) and winds (arrows; unit: m s^{-1}) at 200 hPa, (b)–(c) relative humidity (shading; unit: %), geopotential height (blue contours; unit: dagpm) and winds (arrows; unit: m s^{-1}) at (b) 500 hPa and (c) 850 hPa at 19:00 LST 14 May 2021. The blue stars in panels (a)–(c) denote the location of observed tornado.

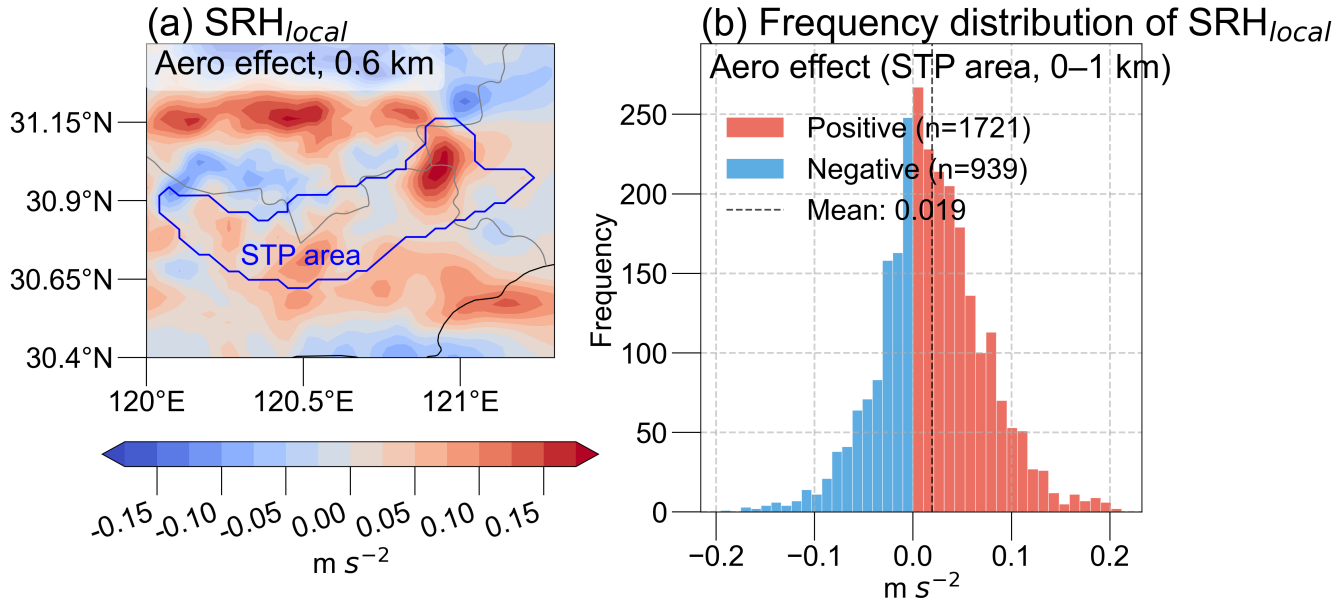

Figure S2. Variations in (a) SRHlocal (shaded; unit: m s^{-2}) due to Aero effect at 0.6 km and 19:00 LST. In panel (a), the blue contour indicates the tracked STP area. Variations in (b) the frequency distribution of SRHlocal due to Aero effect within the tracked STP area in the 0–1 km layer. In panel (b), positive and negative values are shown in red and blue, respectively, with 1,721 positive and 939 negative grid points. The dashed vertical line denotes the mean.

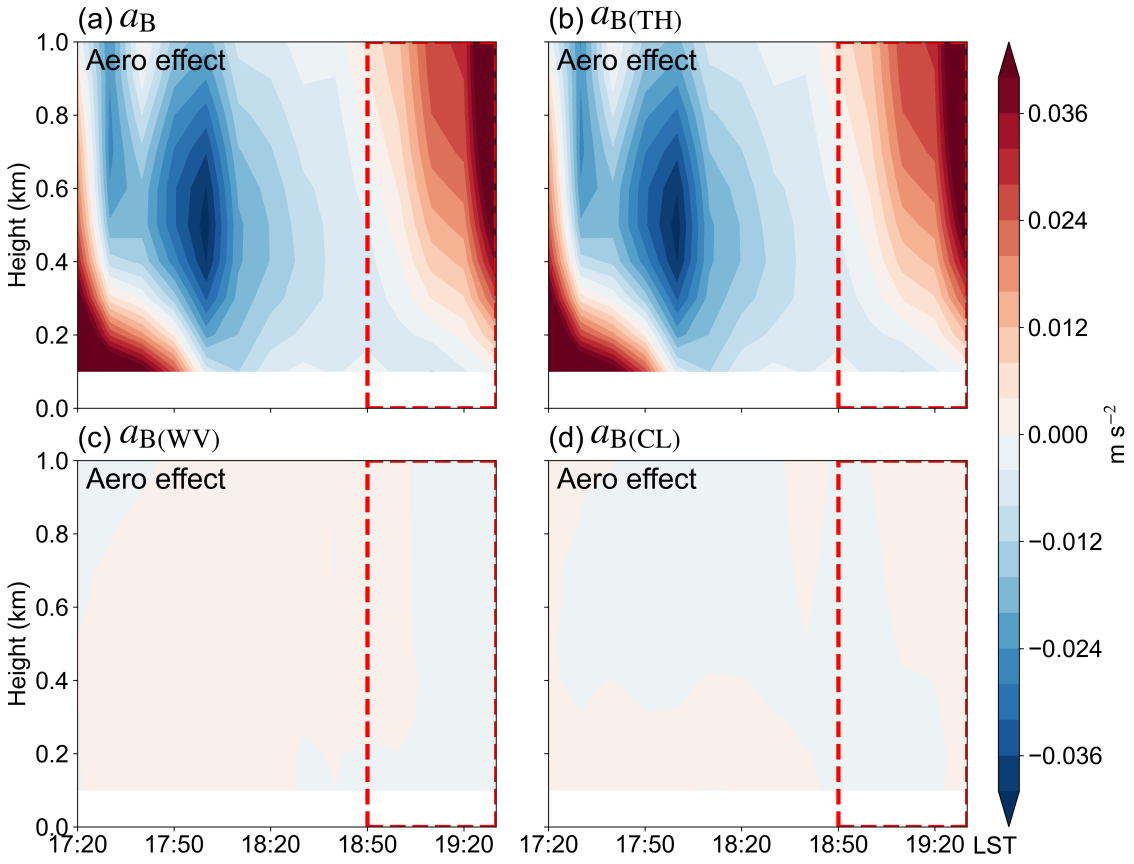

Figure S3. Time–height cross-sections of variations in (a) buoyant acceleration (a_B), (b) thermal buoyant acceleration ($a_{B(\mathrm{TH})}$), (c) water-vapor buoyant acceleration ($a_{B(\mathrm{WV})}$), and (d) condensate loading acceleration ($a_{B(\mathrm{CL})}$) due to Aero effect. All acceleration terms are in units of m s^{-2}. The red dashed rectangles highlight the focus window from 18:50 to 19:30 LST.

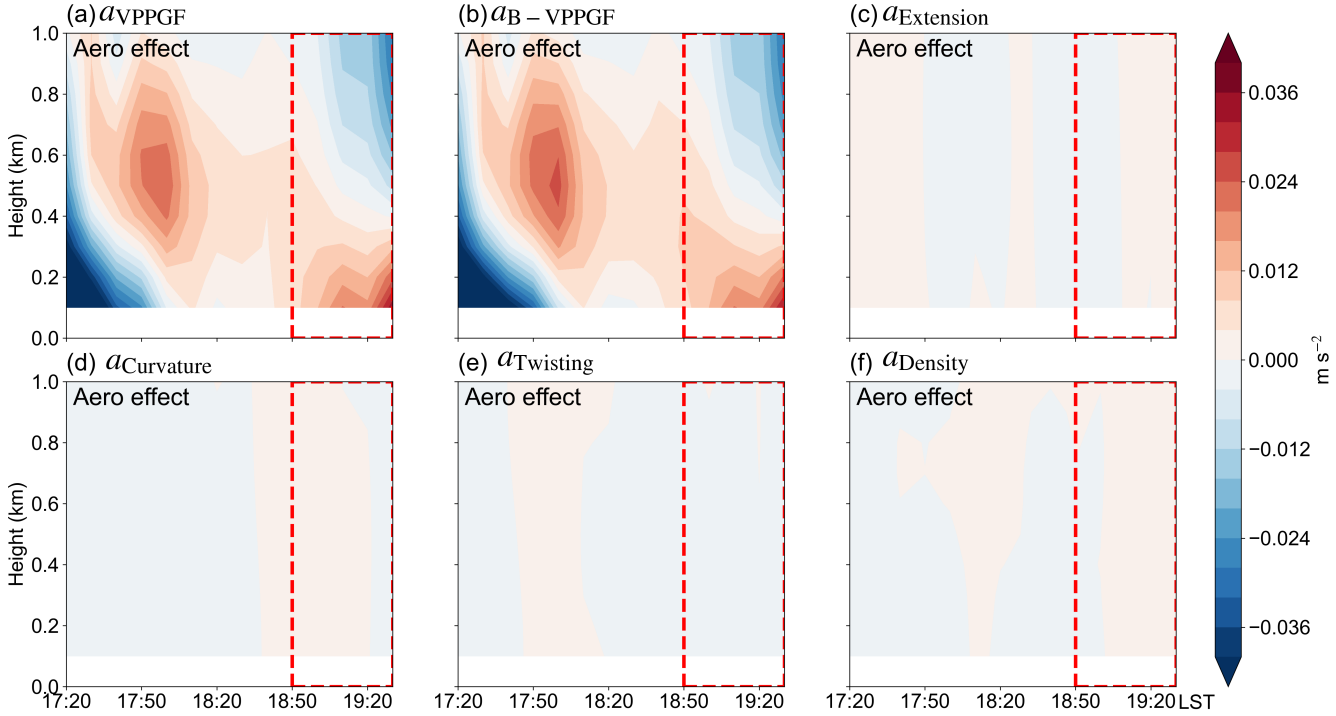

Figure S4. Time–height cross-sections of variations in acceleration due to (a) vertical perturbation pressure-gradient force (a_{VPPGF}), (b) buoyancy-induced vertical perturbation pressure-gradient force ($a_{B\text{-VPPGF}}$), (c) fluid-extension ($a_{\mathrm{Extension}}$), (d) horizontal-curvature ($a_{\mathrm{Curvature}}$), (e) vertical-twisting (a_{Twisting}), and (f) vertical-velocity–density term (a_{Density}) due to Aero effect. All acceleration terms are in units of m s^{-2}. The red dashed rectangles highlight the focus window from 18:50 to 19:30 LST.

References

Chen, F. and Dudhia, J.: Coupling an advanced land surface–hydrology model with the Penn State–NCAR MM5 modeling system. Part I: Model implementation and sensitivity, Mon. Wea. Rev., 129, 569–585, https://doi.org/10.1175/1520-0493(2001)129<0569:CAALSH>2.0.CO;2, 2001.

Didan, K.: MODIS/Terra vegetation indices 16-day L3 global 250 m SIN grid V061, NASA Land Processes Distributed Active Archive Center [data set], accessed: 15 Jan 2026, https://doi.org/10.5067/MODIS/MOD13Q1.061, 2021.

Ek, M. B., Mitchell, K. E., Lin, Y., Rogers, E., Grunmann, P., Koren, V., Gayno, G., and Tarpley, J. D.: Implementation of Noah land surface model advances in the National Centers for Environmental Prediction operational mesoscale Eta model, J. Geophys. Res.-Atmos., 108, 8851, https://doi.org/10.1029/2002JD003296, 2003.

Fan, J., Zhou, Y., Xu, X., Jiang, P., and Li, Z.: MEIC emission-inventory to WRF-Chem grid interpolation and allocation software (Version 1.0), National Copyright Administration of the People's Republic of China [software], Software copyright registration No. 2020SR0414107 accessed: 15 Jan 2026, https://gitee.com/jinfan0931/meic2wrf, 2020.

Geng, G., Liu, Y., Liu, Y., Liu, S., Cheng, J., Yan, L., Wu, N., Hu, H., Tong, D., Zheng, B., Yin, Z., He, K., and Zhang, Q.: Efficacy of China's clean air actions to tackle PM2.5 pollution between 2013 and 2020, Nat. Geosci., 17, 987–994, https://doi.org/10.1038/s41561-024-01540-z, 2024.

Guenther, A.: MEGANv2.1 1km2 global monthly LAIv for 2003, https://doi.org/10.5281/zenodo.10521585, 2024.

Guenther, A. B., Jiang, X., Heald, C. L., Sakulyanontvittaya, T., Duhl, T., Emmons, L. K., and Wang, X.: The Model of Emissions of Gases and Aerosols from Nature version 2.1 (MEGAN2.1): an extended and updated framework for modeling biogenic emissions, Geosci. Model Dev., 5, 1471–1492, https://doi.org/10.5194/gmd-5-1471-2012, 2012.

Iacono, M. J., Delamere, J. S., Mlawer, E. J., Shephard, M. W., Clough, S. A., and Collins, W. D.: Radiative forcing by long-lived greenhouse gases: Calculations with the AER radiative transfer models, J. Geophys. Res.-Atmos., 113, D13 103, https://doi.org/10.1029/2008JD009944, 2008.

Li, M., Liu, H., Geng, G., Hong, C., Liu, F., Song, Y., Tong, D., Zheng, B., Cui, H., Man, H., Zhang, Q., and He, K.: Anthropogenic emission inventories in China: a review, Natl. Sci. Rev., 4, 834–866, https://doi.org/10.1093/nsr/nwx150, 2017.

Morrison, H. and Gettelman, A.: A new two-moment bulk stratiform cloud microphysics scheme in the Community Atmosphere Model, version 3 (CAM3). Part I: Description and numerical tests, J. Climate, 21, 3642–3659, https://doi.org/10.1175/2008JCLI2105.1, 2008.

Nakanishi, M. and Niino, H.: An improved Mellor–Yamada level-3 model: Its numerical stability and application to a regional prediction of advection fog, Boundary Layer Meteorol., 119, 397–407, https://doi.org/10.1007/s10546-005-9030-8, 2006.

National Centers for Environmental Prediction, National Weather Service, NOAA, U.S. Department of Commerce: NCEP FNL Operational Model Global Tropospheric Analyses, continuing from July 1999, NSF National Center for Atmospheric Research [data set], https://doi.org/10.5065/D6M043C6, 2000.

Tilmes, S., Emmons, L. K., Buchholz, R. R., and The CESM2 Development Team: CESM2.2 CAM-chem as Boundary Conditions, NSF National Center for Atmospheric Research [data set], https://doi.org/10.5065/XS0R-QE86, last access: 20 Feb 2026, 2022.

Zaveri, R. A. and Peters, L. K.: A new lumped structure photochemical mechanism for large-scale applications, J. Geophys. Res.-Atmos., 104, 30 387–30 415, https://doi.org/10.1029/1999JD900876, 1999.

Zaveri, R. A., Easter, R. C., Fast, J. D., and Peters, L. K.: Model for Simulating Aerosol Interactions and Chemistry (MOSAIC), J. Geophys. Res.-Atmos., 113, D13 204, https://doi.org/10.1029/2007JD008782, 2008.